J. Fluid Mech. (1981), *vol.* 109, *pp.* 311–337
Printed in Great Britain

Particle motions near the bottom in turbulent flow in an open channel. Part 2

By B. MUTLU SUMER
Technical University of Istanbul, Faculty of Civil Engineering, Taşkişla, Taksim, Istanbul, Turkey
AND ROLF DEIGAARD
Technical University of Denmark, Institute of Hydrodynamics and Hydraulic Engineering, DK-2800, Lyngby, Denmark

(Received 31 March 1980 and in revised form 30 August 1980)

This study continues the investigation of particle motions near the bottom in a turbulent open channel flow, reported by Sumer & Oğuz (1978; hereafter referred to as part 1). Paths of suspended heavy particles were recorded in three dimensions and in time, employing a stereo-photogrammetric system coupled with a stroboscope. In the case of smooth bottom, the measured kinematical quantities concerning the particle motions were found to be in accord with the available information on the 'bursting process'. Agreement between the particle motion and the bursting process provided further support for the mechanism of particle suspension near the bottom proposed in part 1. Similar experiments were carried out when the bottom was rough. Comparison between the smooth- and rough-bottom cases could be made on the same basis as the flow Reynolds number as well as the particle properties were kept almost unchanged in both the smooth and rough boundary experiments. The observations showed that particle motions close to the rough bottom are very similar in character to those in the smooth-bottom case. The findings of the present paper suggested that the suspension mechanism given for the smooth-boundary flow could be extended to the rough-boundary case.

1. Introduction

If the correct conditions exist, a small heavy particle released into a channel flow is prevented from settling on the bottom; it travels most of the time close to the bottom of the channel. The mechanism which prevents the particle from settling should be closely associated with the turbulence structure near the bottom, namely the bursting process.

Sutherland (1967) explained particle 'entrainment' by turbulent flows by making use of turbulence observations near the bed. A critical review of Sutherland's work can be found in Sumer & Oğuz (1978). Engelund (1970) discussed a possible mechanism of particle suspension. Engelund's work has been discussed in some detail in part 1. Jackson (1976) noted that 'a plausible candidate for the suspension mechanism is the bursting process', presenting a review of scattered observations on sediment dispersal from the bed which provided qualitative support for his suggestion.

An interesting argument comes from Lumley's (1978, p. 309) review. In the case of

a boundary layer above a horizontal wall in which heavy, 'inertia-free' particles are suspended, the vertical component of particle mean velocity, $\bar{v}_p$, must be essentially zero since the particle cannot penetrate the wall or leave the top of the boundary layer. Pointing out that, for heavy, 'inertia-free' particles, the relation $v_p = v - w$ holds at any instant, Lumley reached the conclusion that the vertical component of fluid velocity seen by the particle (on the average), i.e. $\bar{v}$, must be equal to w since $\bar{v}_p = 0$, where w is the particle settling velocity. This means that the particle must seek out (on the average) rising currents, to compensate the tendency to fall out. After having come to the latter conclusion, Lumley continued his discussion saying, that no measurements have been made but in all likelihood the particles which fall to the bottom are swept into spaces between the longitudinal big eddies and are lifted and ejected into the upper part of the layer by the updraft (and associated 'bursting' phenomenon) between them, and adding that this sort of behaviour may be seen in dry snow flakes on a hard-surface road, or in sand blowing across a beach.

Grass (1974) filmed the process of suspension of sand particles in a turbulent boundary layer on a flat plate. His ciné film revealed most of the details of the flow structure (visualized by the sand) shown up by earlier visualization observations (e.g. Grass 1971; Nychas, Hershey & Brodkey 1973; Offen & Kline 1973; and others) and thus directly established the link between the particle suspension and the bursting process.

In part 1 of this study, Sumer & Oğuz (1978) made observations of the motion of heavy suspended particles near the smooth bottom in turbulent flow in an open channel. The kinematical quantities concerning the particle motion obtained through the path records appeared to be in accord with those of the earlier visualization observations, which led the authors to make an attempt to explain the mechanism of particle suspension close to the wall in turbulent flows in terms of the bursting process.

Investigation of motions of small heavy particles near a rough bottom in turbulent channel flows has far greater importance than the smooth bottom case as the former is encountered more often in practice. Despite the fact that we have gained considerable insight into the structure of turbulence near a smooth-wall recently, this is not so for the rough-wall case; thus, the lack of information in the case of rough wall makes it even more difficult to understand the responsible mechanism of particle suspension in the latter case. The papers of Grass (1971) and Nakagawa & Nezu (1977, 1978) appear to be the only ones in the literature studying the effect of the wall roughness upon the near-wall turbulence structure in the 'modern' sense; both works suggested that a quasi-cyclic flow pattern, the bursting process, occurs near the wall in a turbulent boundary layer, irrespective of the wall roughness.

Abbott & Francis (1977) photographed the paths of solid grains in an open water channel with a rough bottom, employing a multi-exposure technique; the photographs taken were then analysed to determine the position, velocities and accelerations of grains. The relevance of the Abbott & Francis study to the present work is discussed in some detail in § 5.

The objective of the present study is (*a*) to make further observations of the motion of heavy suspended particles near the bottom in turbulent flow in an open channel (1) when the bottom is smooth and (2) when it is rough; and (*b*) to test the suspension mechanism given in part 1 against the new data obtained in the present study. To this end, a stereo-photogrammetric system was used to record the three-dimensional

motion of single particles. The photogrammetric system as well as the flow and particle properties are described in the next section. Results of the smooth and rough bottom experiments are described in § 3 and § 4 respectively. The findings of the present study are discussed in § 6.

2. Experimental facility

2.1. *The flow*

The $0{\cdot}30 \times 0{\cdot}30 \times 10$ m flume used in the experiments is located in the laboratory of the Institute of Hydrodynamics and Hydraulic Engineering, Technical University of Denmark. It has glass side walls and its slope is adjustable. Water was recirculated through the flume via a water tank, a pump, and a returning pipe. The rate of flow was controlled by means of a valve and measured using an orifice meter which was fixed to the returning pipe. The flow depth was adjusted by means of a weir and measured using a pointer gauge.

The rough-bottom experiments were performed in the same flume used for the smooth bottom experiments. Rough bottom conditions were achieved by covering the flume bed with 3·6 mm pebbles of fairly uniform size and glued one layer deep to the flume bed. The roughness Reynolds number was $ku_*/\nu = 81$, where u_* is the shear velocity, k is the mean height of roughness tops above base plate, and ν is the kinematic viscosity.

The depth of flow was kept constant at 6·8 cm (in the smooth-bottom case) and 7·0 cm (in the rough-bottom case) in the region of the working section located between the distances 5 m and 7·5 m downstream from the flume inlet, the depth being measured from the theoretical bottom in the rough-bottom case. The energy grade line down the flume gave rise to a small difference of 3 % in depth between the upstream and downstream ends of the working section. This divergence from strictly uniform flow conditions was considered to be sufficiently small to be ignored for the purposes of the present work. The mean flow velocity was calculated from the volumetric discharge divided by the cross-sectional area and kept constant throughout the tests at approximately 29·8 cm s^{-1} in the smooth-bottom case and 29·1 cm s^{-1} in the rough-bottom case. The flow Reynolds number, based on the mean flow velocity and the depth, was approximately 21 000. The shear velocity was predicted from the measured velocity profiles and found to be 1·44 cm s^{-1} and 2·19 cm s^{-1} in the smooth- and rough-bottom cases respectively. In the case of smooth bottom, the preceding value was found to agree to within 4–5 % with the values obtained by using the Darcy–Weisbach equation $u_* = (f/8)^{\frac{1}{2}}U_m$, where $f = 0{\cdot}316/Re^{\frac{1}{4}}$ (since $Re < 10^5$; Henderson 1966, p. 93). Here Re is the Reynolds number, based on the mean flow velocity and hydraulic radius: $Re = 4RU_m/\nu$.

To flatten the lateral velocity profile, two rows of vertical rods of 7 mm (the rods being 1·5 cm apart for the upstream row and 3 cm apart for the downstream row, and the rows themselves being 2·5 cm apart) were fixed 3·1 m downstream from the flume inlet; in fact, various combinations of the rods and their locations were tried to achieve this goal, measuring the mean streamwise velocity by traversing a miniflowmeter across the flume at five heights (from 1 cm to 5 cm) above the bottom at three stations (1·25 m apart). The velocity measurements showed that, with the above arrangement of rods, the local mean streamwise velocity varied by 3 % on the average (with a

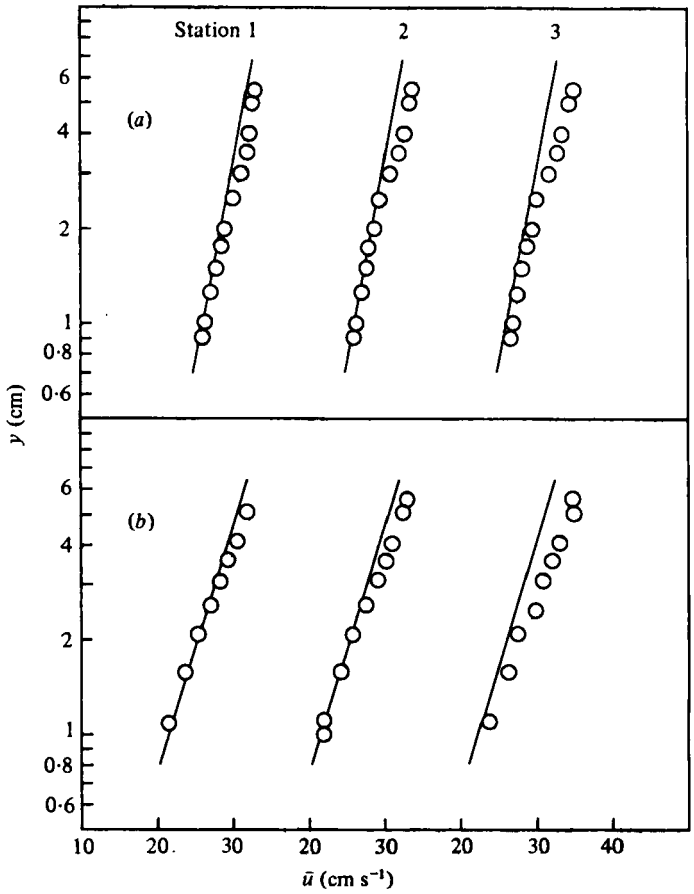

FIGURE 1. Mean velocity profiles along the centre-line of the working section. Stations 1 and 3 respectively are located 5 m and 7·5 m downstream from the flume inlet and station 2 in between. (*a*) Smooth bottom. (*b*) Rough bottom. Straight lines, logarithmic velocity profiles.

maximum of 5%) in the smooth-bottom case and by 7% on the average (with a maximum of 12%) in the rough-bottom case over the centre 20 cm of the flume width. Mean velocity profiles in the vertical along the centre-line of the working section are plotted in figure 1 accompanied by the corresponding logarithmic profiles (Monin & Yaglom 1971, pp. 270–295) $\bar{u} = u_*(2{\cdot}4 \ln y^+ + 5{\cdot}8)$ and $\bar{u} = 2{\cdot}5\, u_* \ln(30y/k_s)$ for the smooth- and rough-boundary cases respectively. Here, $y^+ = yu_*/\nu$, y is the distance from the bottom in the smooth-bottom case and that from the theoretical bottom in the rough-bottom case, and k_s is the equivalent sand roughness. Note that in the smooth-boundary case, roughness elements were fixed on the bottom at the inlet to make the flow fully developed as close to the flume inlet as possible.

In the rough-wall case, the location of the theoretical bottom was obtained by shifting the origin of y to yield the best straight line on a series of semi-log plots of the mean velocity data and found to lie at a distance of about $0{\cdot}25k$ below the roughness tops. Note that in this procedure only those parts of the velocity data which correspond to $y/h < 0{\cdot}25$ were taken into account since the deviation from the logarithmic equation begins at about $y/h = 0{\cdot}25$ (Monin & Yaglom 1971, p. 304). As has been

Bottom	Flow depth h (cm)	Mean flow velocity U_m (cm s^{-1})	$Re = hU_m/\nu$	Shear velocity u_* (cm s^{-1})	Mean roughness height k (mm)	ku_*/ν
Smooth	6·8	29·8	21000	1·44	0	0
Rough	7·0	29·1	21000	2·19	3·6 mm pebbles	81

TABLE 1. Flow properties.

Particle	Particle size d (mm)	Particle size du_*/ν	Settling velocity w (cm s^{-1})	Water temperature T (°C)	Specific gravity s	Settling velocity parameter† $w/(\kappa u_*)$
			Bottom smooth			
A (slightly heavier than water)	2·9	44	0·64	23·4	1·0029	1·0 (5)
B (moderately heavier than water)	3·0	46	1·33	23·3	1·0075	2·2
C (considerably heavier than water)	3·1	47	3·06	22·3	1·0258	5·1
			Bottom rough			
D (moderately heavier than water)						
Run *D*1	3·0	67	1·49	21·4	1·0090	1·6
Run *D*2	3·0	67	1·41	22·2	1·0081	1·5

† κ (the Kármán constant) is taken to be 0·42.

TABLE 2. Particle properties.

mentioned above, the shear velocity was predicted from the slope of the semi-log plot of the mean velocity data. The $\bar{u}$-intercept of the latter gave the equivalent sand roughness to be about 0·5 cm. A summary of the flow properties is given in table 1.

2.2. *The particles*

Of the factors which were taken into account in choosing the particles, the most important one was the need for the particles to stay in suspension. To meet this requirement of particles with extremely small settling velocities, we produced them ourselves. The particles were made of plastic, being slightly heavier than water (yet being too heavy for our purposes). The material was shaped into spherical form of the required size. A fine hole was drilled in the particle and tiny pieces of 'expanded polyester' were driven into it. The hole was then sealed with bees' wax. This procedure made it possible to have particles with extremely small settling velocities. More information about the factors which were taken into account in choosing the particles can be found in Sumer & Deigaard (1979).

Three types of particles were used in the smooth bottom experiments. One was

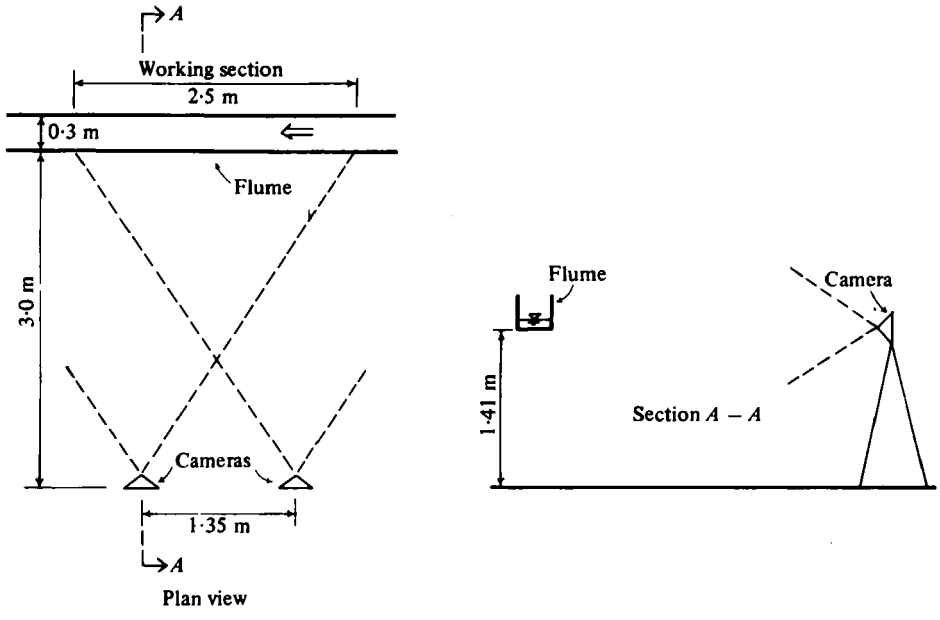

FIGURE 2. The camera set-up.

slightly heavier than water (particle A), the other was moderately heavier than water (particle B), and the third was considerably heavier than water (particle C). All had almost the same size. Although the particle C did not quite satisfy the requirement that the particles should stay in suspension, it was purposely chosen so as to get an insight into what is occurring in this case. As to the rough-bottom experiments, only one type of particle was used since the specific object of these experiments was to get an insight into the mechanics of particle motions in the case of rough-boundary flow. The particle used in the latter tests was moderately heavier than water. The particle is designated with the letter D. With particle D, two runs were conducted: run $D1$ and run $D2$. The particle properties are given in table 2.

2.3. *The photographic technique*

The photographic technique involves a stereo-photogrammetric method (developed at the Institute of Landsurvey and Photogrammetry, Technical University of Denmark) which made it possible to record particle paths in three dimensions. The experimental set-up is shown schematically in figure 2. The cameras viewed the working section through the glass side of the flume.

The following experimental procedure was adopted in particle photographing. A particle was released into the flow through a simple ⊥- shaped tube located close to the flume inlet. A stroboscope was activated in the dark, illuminating the particle from the top and following it throughout its path. The flash frequency of the stroboscope was 11·6 Hz. At the instant when the particle entered the working section, the shutters of the cameras were opened and maintained continuously at this position until the particle left the working section. This arrangement made it possible to record the side-view motion of the particle as a series of dots on film plates, the dots being

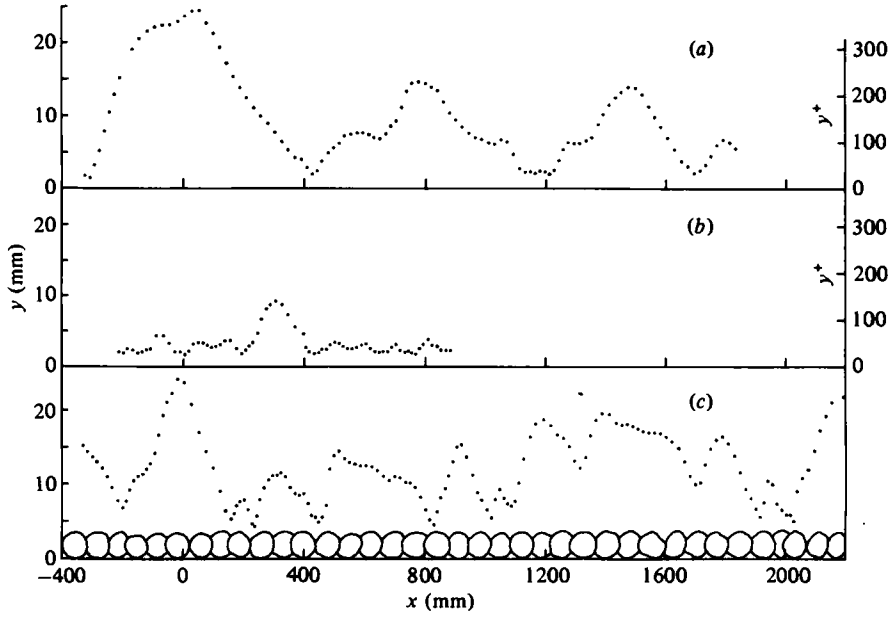

FIGURE 3. Typical paths of individual particles in side view. Flow from left to right. (*a*) Particle *A* (run no. S03–01); smooth bottom. (*b*) Particle *C* (run no. S01–08); smooth bottom. (*c*) Particle *D* (run *D*1, run no. R04–08); rough bottom. Dots are spaced 0·086 s apart. The vertical scale is considerably exaggerated.

spaced 1:11·6 Hz = 0·086 s apart (see figure 3). The particle was retrieved at the downstream end of the flume. One such particle was used repeatedly.

Film readings were made for some 50 pairs of film plates at the Institute of Landsurvey and Photogrammetry, Technical University of Denmark, and lists of printed x, y and z co-ordinates of the particle images were obtained. The mean errors in the x, y and z co-ordinates were estimated to be 0·12 mm, 0·12 mm and 0·28 mm respectively. For more information about the photogrammetric method employed in this study, see Jacobi (1979), which was reproduced in Sumer & Deigaard (1979).

2.4. *Miscellaneous*

Uncertainties in various quantities of interest are estimated to be as follows: uncertainty in the flow rate = $\pm 0{\cdot}005\,\mathrm{l\,s^{-1}}$ for the smooth-bottom case and $\pm 0{\cdot}009\,\mathrm{l\,s^{-1}}$ for the rough-bottom case, that in the flow depth = $\pm 0{\cdot}07$ cm, that in the mean flow velocity = $\pm 0{\cdot}3\,\mathrm{cm\,s^{-1}}$, and that in the shear velocity = $\pm 0{\cdot}01\,\mathrm{cm\,s^{-1}}$ for the smooth-bottom case and $\pm 0{\cdot}1\,\mathrm{cm\,s^{-1}}$ for the rough-bottom case. The uncertainties involved in co-ordinate measurements of particle images on film plates have already been given in the preceding section. In the smooth bottom experiments, the distance from the bottom of the particle is expressed in terms of y^+. The uncertainty in y^+ is estimated to be ± 2.

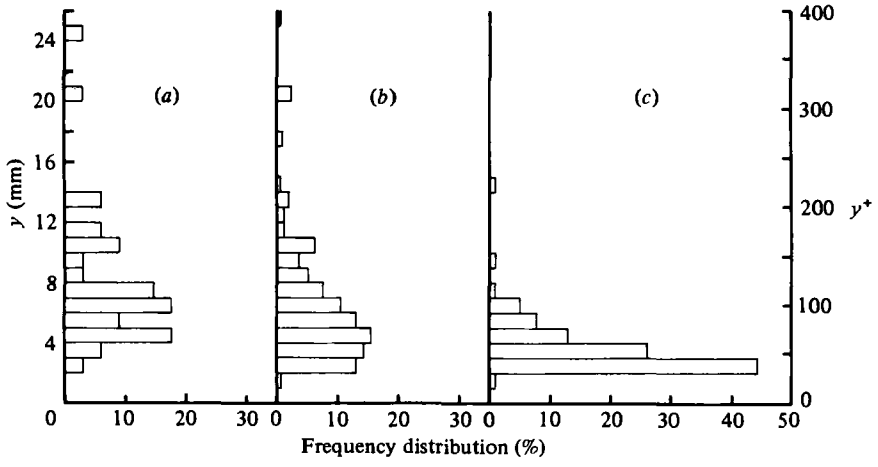

FIGURE 4. Frequency histograms of y^+ at termination of the upward paths of individual particles, y^+ at the origin of the upward paths being in the wall region. (*a*) Particle *A*, $\bar{y} = 8{\cdot}1$ mm ($\bar{y}^+ = 125$), $\sigma_y = 4{\cdot}6$ mm ($\sigma_{y^+} = 71$), $N = 34$. (*b*) Particle *B*, $\bar{y} = 6{\cdot}7$ mm ($\bar{y}^+ = 103$), $\sigma_y = 4{\cdot}3$ mm ($\sigma_{y^+} = 66$), $N = 161$. (*c*) Particle *C*, $\bar{y} = 3{\cdot}6$ mm ($\bar{y}^+ = 54$), $\sigma_y = 1{\cdot}7$ mm ($\sigma_{y^+} = 26$), $N = 115$. N denotes the sample size.

3. Presentation of the smooth-bottom results

For convenience, throughout the presentation, particle positions in the vertical and also displacements of particles will often be expressed in terms of wall parameters u_* and ν; i.e. y^+ where $y^+ = yu_*/\nu$. In this section and thereafter, the region $5 < y^+ < 70$ where most of the turbulence activity takes place will be called the wall region.

3.1. *Particle paths*

In this subsection, a description of the observed particle paths is given: three typical path records in side-view are shown in figure 3. As is seen, the path of an individual particle consists of an alternation between upward and downward paths traced by the particle as it travels close to the bottom. The common feature in all path records obtained in the present experiments is that most of the downward motions of particles coming close to the bottom terminated at a y^+ in the wall region, or sometimes at the flume bottom.† This suggests us to begin the description of the observed paths of particles with a particle which starts to travel upwards from the wall region.

Figure 4 shows frequency histograms of y^+ at the termination of the upward paths of individual particles, y^+ at the origin of the upward paths being in the wall region. The statistical properties of y^+ at termination of the upward paths are given in table 3. Table 3 also gives other statistics of the upward paths where X and Z respectively are the streamwise and transverse distances travelled by an individual particle as it rises from the wall region until its upward motion terminates, and T is the time between the instant an individual particle starts to rise and the instant its upward motion terminates, i.e., the 'rise' time (see figure 6). Note that, for comparison, the quantities X and Z are non-dimensionalized by wall parameters u_* and ν, and the quantity T by

† The distance of the centroid of the particle from the bottom is about $y^+ = 23$ when the particle touches the bottom.

Particle	Mean and s.d. of y position at terminations of upward paths: $\bar{y}$ (mm)	$\bar{y}^+$	σ_y (mm)	σ_{y+}	Mean and s.d. of streamwise displacements: $\bar{X}$ (mm)	$\bar{X}^+$	σ_X (mm)	σ_{X+}	s.d. of transverse displacements: σ_Z (mm)	σ_{Z+}	Mean 'rise' time: $\bar{T}$ (s)	$\frac{\bar{T}u_\infty}{h}$	Sample size N
(1)	(2)	(3)	(4)	(5)	(6)	(7)	(8)	(9)	(10)	(11)	(12)	(13)	(14)
A	8·1	125	4·6	71	132	2000	91	140	8·3	128	0·63	3·0	34
B	6·7	103	4·3	66	104	1600	75	115	6·4	98	0·51	2·4	161
C	3·6	54	1·7	26	39	590	30	45	3·6	54	0·23	1·1	115

TABLE 3. Statistical properties of upward paths of individual particles, y^+ positions at the origins of the paths being in the wall region. s.d. denotes the standard deviation.

Particle	n_{total}	n_{back}	% total particles returning back to the wall region $\frac{n_{back}}{n_{total}}$	Mean and s.d. of y^+ position at terminations of downward paths: $\bar{y}$ (mm)	$\bar{y}^+$	σ_y (mm)	σ_{y+}	Mean time spent by particle as it traces its subsequent upward and downward paths: $\bar{T}_1$ (s)	$\frac{\bar{T}_1 u_\infty}{h}$	Mean streamwise distance travelled by particle as it traces its subsequent upward and downward paths: $\bar{X}_1$	$\frac{\bar{X}_1}{h}$	Sample size, N
(1)	(2)	(3)	(4)	(5)	(6)	(7)	(8)	(9)	(10)	(11)	(12)	(13)
A	34	21	62	2·6	40	0·9	14	1·09	5·3	234·8	3·5	21
B	161	124	77	2·5	38	0·6	9	0·91	4·4	187·8	2·8	124
C	115	107	93	2·2	33	0·4	6	0·42	2·0	73·4	1·1	107

TABLE 4. Statistical properties of downward paths of those particles which return back to the wall region after completing their upward paths whose origins are in the wall region. n_{total} = total number of particles, upward paths of which originated in the wall region. n_{back} = Of the n_{total} particles, number of those which return back to the wall region. s.d. denotes standard deviation.

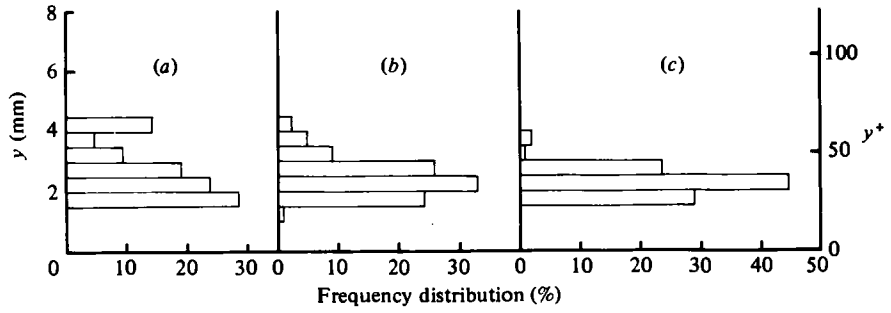

FIGURE 5. Frequency histograms of $\bar{y}^+$ at termination of the downward paths of those particles which return back to the wall region, after completing their upward paths. (*a*) Particle *A*, $\bar{y} = 2{\cdot}6$ mm ($\bar{y}^+ = 40$), $\sigma_y = 0{\cdot}9$ mm ($\sigma_{y^+} = 14$), $N = 21$. (*b*) Particle *B*, $\bar{y} = 2{\cdot}5$ mm ($\bar{y}^+ = 38$), $\sigma_y = 0{\cdot}6$ mm ($\sigma_{y^+} = 9$), $N = 124$. (*c*) Particle *C*, $\bar{y} = 2{\cdot}2$ mm ($\bar{y}^+ = 33$), $\sigma_y = 0{\cdot}4$ mm ($\sigma_{y^+} = 6$), $N = 114$. N denotes the sample size.

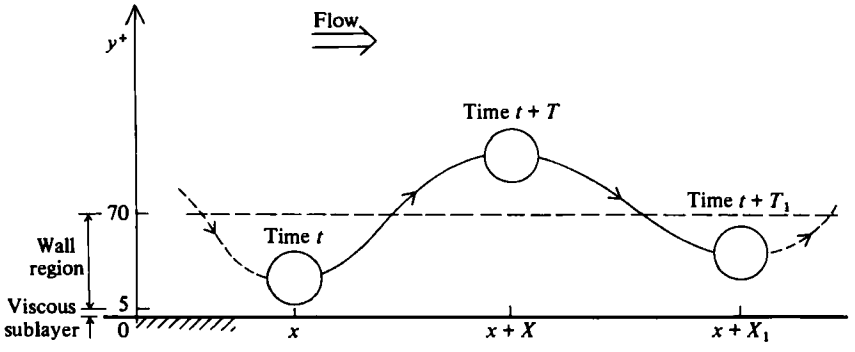

FIGURE 6. A complete cycle of particle path in side view.
t = time, T = burst duration, T_1 = burst periodicity.

the outer flow parameters u_∞ (the maximum velocity) and h (the flow depth). The relevant discussion will be given later in §5.

The particles whose upward paths originate in the wall region start to return towards the bottom as their upward paths terminate. Of the particles returning towards the wall, some could penetrate to the wall region (figure 6); but some could not penetrate there, their downward paths terminating in the outer region $y^+ > 70$. Column 4 of table 4 gives the percentage of the total number of particles returning to the wall region. The significance of these figures will be discussed later in §5. Figure 5 illustrates the frequency histograms of y^+ at termination of the downward paths of those particles which return back to the wall region. The statistical properties of y^+ at termination of the downward paths are given in table 4. In table 4 other relevant statistics are also given: T_1, the time spent by the particle as it traces its subsequent upward and downward paths, and X_1, the streamwise distance travelled by the particle during the time period T_1; y^+ at the origin of the upward path and y^+ at the termination of the downward path, both being in the wall region (see figure 6).

For more information about the path statistics obtained in the present work, the reader is referred to Sumer & Deigaard (1979).

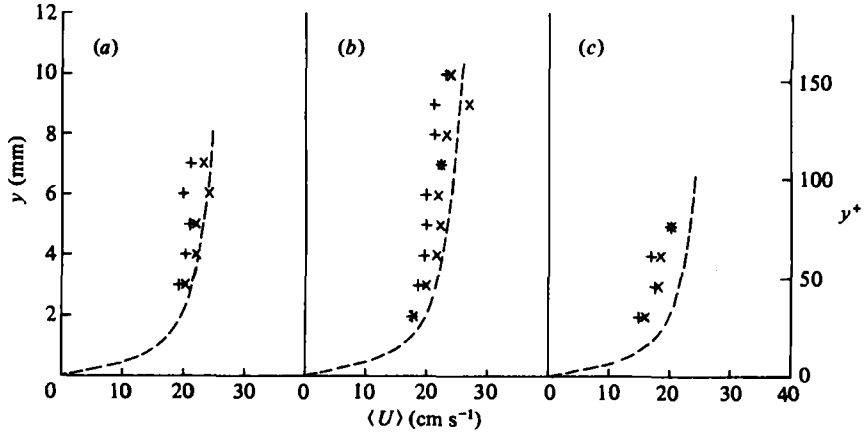

FIGURE 7. Longitudinal velocity data. (*a*) Particle *A*; (*b*) particle *B*; (*c*) particle *C*. +, $\langle U \rangle$ corresponding to upward paths; ×, $\langle U \rangle$ corresponding to downward paths; – – –, the logarithmic velocity profile $\bar{u} = u_* (2{\cdot}4 \ln y^+ + 5{\cdot}8)$.

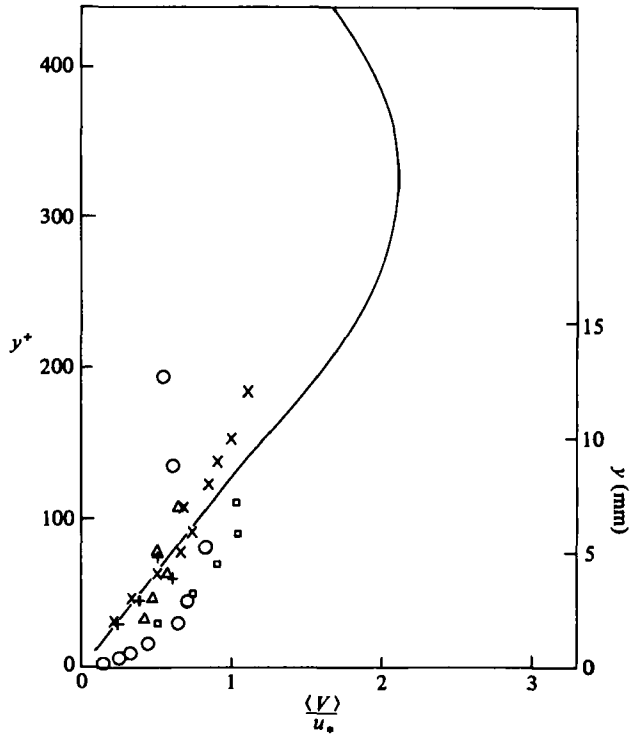

FIGURE 8. Vertical velocity data corresponding to upward paths (ejection velocity data). Mean of the sample of V velocities at a particular depth increment. △, particle *A*, ×, particle *B*; +, particle *C*; □, Sumer & Oğuz (1978, figure 6); ——, Grass (1974), mean ejection velocities of fine sand particles; ○, Brodkey *et al.* (1974, figure 11), mean of the velocity component normal to the wall corresponding to ejection type of motion.

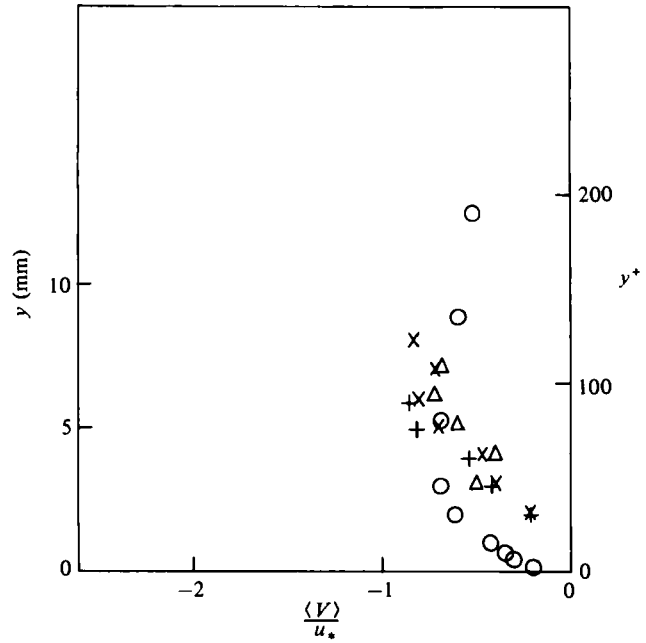

FIGURE 9. Vertical velocity data corresponding to downward paths. Mean of the sample of V velocities at a particular depth increment. △, particle A; ×, particle B; +, particle C; ○, Brodkey *et al.* (1974, figure 11), mean of the velocity component normal to the wall corresponding to sweep type of motion.

3.2. *Particle velocities*

Data on particle velocities over both upward and downward paths of particles are presented in this section; again, here too, both y^+ at the origin of the upward paths and y^+ at the termination of downward paths are in the wall region; i.e., the path pattern over which the velocities are predicted is that as given in figure 6.

The longitudinal and vertical components of particle velocity are denoted by U and V respectively. Here U is an average velocity in the sense that it was predicted as the average value, over the upward path or the downward path, of the longitudinal velocity of particle. Similarly, V is the average value, over the upward path or the downward path, of the vertical velocity of particle. It is assumed that these average velocities occurred at $\bar{y}^+ = \frac{1}{2}(y^+_{or} + y^+_t)$, where y^+_{or} and y^+_t are y^+ at the origin and y^+ at the termination of the particular upward (or downward) path respectively.

For the sake of clarity, the U-velocity data obtained were plotted in the following manner as there were some 30 $(U, \bar{y}^+)$ pairs for particle A, 140 pairs for particle B and 110 pairs for particle C in the narrow interval $0{\cdot}2\,\text{cm} < y < 1\,\text{cm}$. Similar considerations apply to the V-velocity data obtained. The interval $0{\cdot}2\,\text{cm} < y < 1\,\text{cm}$ was divided into small increments of $\Delta y = 0{\cdot}1\,\text{cm}$. At each increment, mean values $\langle U \rangle$ and $\langle V \rangle$ of the samples of U and V velocities respectively, were predicted. It is these mean values which are plotted in figures 7–9.

In figure 7 the $\langle U \rangle$ velocity data are plotted against y^+. In figure 8 the $\langle V \rangle$ velocity data are plotted corresponding to upward paths (ejection-velocity data) against y^+ together with the available information. In this figure, Sumer & Oğuz's (1978) data constitute a plot of the $\langle V \rangle$ velocities predicted exactly in the same way as explained in the preceding paragraph; Grass' (1974) data represent the mean ejection velocities

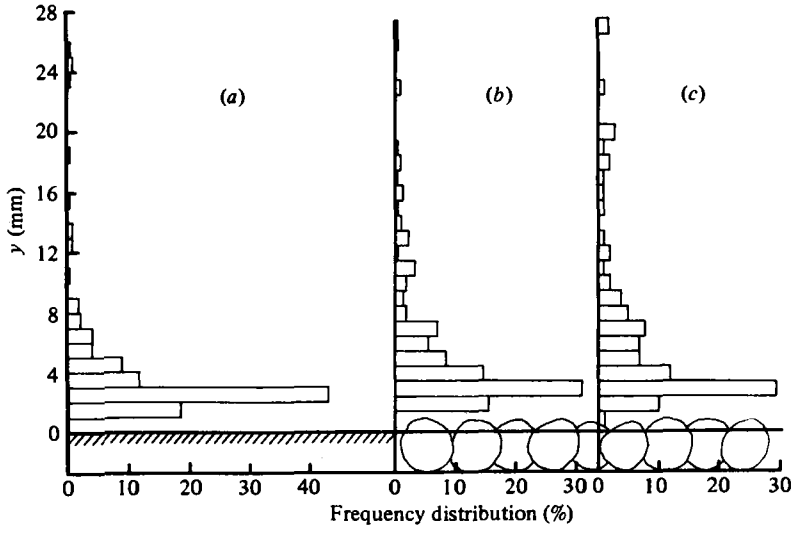

FIGURE 10. Frequency histograms of y at origin of upward paths close to wall. (*a*) Smooth wall (particle B), $\bar{y} = 3{\cdot}9$ mm, $\sigma_y = 3{\cdot}8$ mm, $N = 214$. (*b*) Rough wall (particle D, run $D1$), $\bar{y} = 5{\cdot}3$ mm, $\sigma_y = 4{\cdot}5$ mm, $N = 213$. (*c*) Rough wall (particle D, run $D2$), $\bar{y} = 6{\cdot}5$ mm, $\sigma_y = 6{\cdot}1$ mm, $N = 102$. N denotes the sample size.

of fine sand particles; and Brodkey, Wallace & Eckleman's (1974, figure 11) data represent the mean of the fluid velocity normal to the wall corresponding to an 'ejection type of motion' (see part 1, p. 117 and fig. 6). Figure 9 presents the $\langle V \rangle$ velocity data corresponding to downward paths plotted against y^+ where also Brodkey *et al.* (1974, figure 11) data corresponding to a 'sweep type of motion' are plotted. Of the data of Brodkey *et al.* plotted in figures 8 and 9, those corresponding to $y^+ = 135$ and $y^+ = 195$ seem to be dubious as these y^+ positions were located in the central part of the oil channel used by Brodkey *et al.* (in fact, $y^+ = 195$ corresponds to the centre of the channel, i.e. $y/b = 1$, where b is the half-width of the channel); thus any motion detected at these positions might have been influenced by the bursting process in the other half of the channel.

4. Presentation of the rough-bottom results

In contrast to the case of smooth wall, particle position in the vertical in the rough-bottom case will not be expressed in terms of y^+ ($= yu_*/\nu$) units as the roughness Reynolds number ku_*/ν ($= 81$) falls into the rough boundary category $ku_*/\nu > 70$, thus the viscosity has no effect on the flow.

To facilitate comparison, any result of the rough-bottom case will be accompanied by its counterpart obtained in the smooth-bottom case. Such a comparison is possible, because (*a*) the flow velocity and the flow depth (thus Re number) were kept almost unchanged in both the smooth- and rough-wall tests, and (*b*) the properties of the corresponding particles were also kept almost the same in these two experiments; particle B of the smooth-wall case and the particle used in the rough-wall case (particle D) have almost the same characteristics (see table 2). As has been implied above, the so-called wall region, $y^+ < 70$, practically ceases to exist in the case of rough wall. Thus, to make the comparison between the smooth and rough boundary

Wall	Particle	Mean and s.d. of y at termination; downward paths: $\bar{y}$ (mm)	σ_y (mm)	Mean and s.d. of y at termination; upward paths: $\bar{y}$ (mm)	σ_y (mm)	Mean and s.d. of streamwise displacements: $\bar{X}$ (mm)	σ_X (mm)	s.d. of transverse displacement σ_Z (mm)	Mean and s.d. of 'rise' time: $\bar{T}$ (s)	σ_T (s)	Non-dimensional 'rise time', $\frac{\bar{T}u_\infty}{h}$
(1)	(2)	(3)	(4)	(5)	(6)	(7)	(8)	(9)	(10)	(11)	(12)
Smooth	B	3·9	3·8	8·1	6·1	106·1	85·2	6·6	0·51	0·36	2·4
Rough	D										
	Run $D1$	5·3*	4·5	11·6*	7·7	84·2	74·2	9·1	0·44	0·32	2·0
	Run $D2$	6·5*	6·1	14·4*	10·1	101·7	85·5	7·8	0·49	0·37	2·3

* The y distances are measured from the theoretical bottom (not from the base plate).

TABLE 5. Statistical properties of upward paths of individual particles. s.d. denotes standard deviation.

Wall	Particle	Mean and s.d. of streamwise distance travelled by particle as it traces its subsequent upward and downward paths: $\bar{X}_1$ (mm)	σ_{X_1} (mm)	Non-dimensional $\bar{X}_1$, $\frac{\bar{X}_1}{h}$	Mean and s.d. of time spent by particle as it traces its subsequent upward and downward paths: $\bar{T}_1$ (s)	σ_{T_1} (s)	Non-dimensional $\bar{T}_1$, $\frac{\bar{T}_1 u_\infty}{h}$
(1)	(2)	(3)	(4)	(5)	(6)	(7)	(8)
Smooth	B	211·6	170·8	3·1	0·97	0·66	4·6
Rough	D						
	Run $D1$	176·3	157·2	2·5	0·85	0·58	4·0
	Run $D2$	209·3	180·7	3·0	0·99	0·72	4·6

TABLE 6. Statistical properties of subsequent upward and downward paths. s.d. denotes standard deviation.

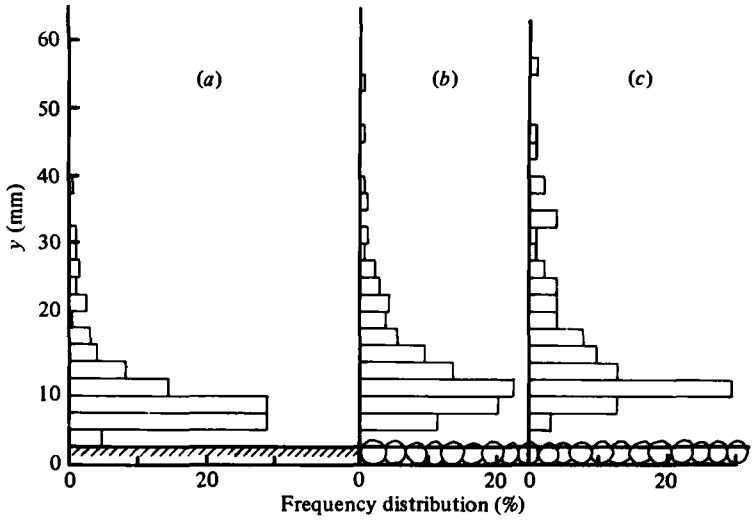

FIGURE 11. Frequency histograms of y at termination of upward paths. (*a*) Smooth wall (particle *B*), $\bar{y} = 8{\cdot}1$ mm, $\sigma_y = 6{\cdot}1$ mm, $N = 207$. (*b*) Rough wall (particle *D*, run *D*1), $\bar{y} = 11{\cdot}6$ mm, $\sigma_y = 7{\cdot}7$ mm, $N = 213$. (*c*) Rough wall (particle *D*, run *D*2), $\bar{y} = 14{\cdot}4$ mm, $\sigma_y = 10{\cdot}1$ mm. $N = 102$. N denotes the sample size.

cases on the same basis, some statistics in connection with the smooth-wall case were re-evaluated, dropping the condition $y^+ < 70$ where the latter had been involved as an extra condition in predicting the conditional statistics in the smooth boundary case. It should be noted that no significant variation was obtained between the re-evaluated statistics and the conditional ones.

4.1. *Particle paths*

Figure 3 shows a typical path record in side-view observed in the case of rough wall. As is seen, the path consists of an alternation between upward and downward paths exactly in the same fashion as that in the case of smooth wall. As in the latter case, most of the downward motions of particle terminate at a position in a narrow y-region close to the wall, or sometimes at the tops of roughnesses, and then the particle starts to rise again.

In figure 10 the frequency histograms of y at the origin of the upward paths close to the bottom are shown. The relevant statistics are given in columns 3 and 4 in table 5. Figure 3 indicates that particles are ejected away to the outer region from a narrow y-region close to the wall, but the ejection region appears to be wider in the case of rough wall (yet it is a small fraction, about 15–20 %, of the total flow depth).

In figure 11 are shown the frequency histograms of y at termination of the upward paths. The relevant statistics are given in table 5. Figure 11 suggests that the particles, in single continuous motions, get much higher elevations (on the average) in the case of rough wall than in the case of smooth wall. Indeed, in the rough wall case of our study, some particles could reach positions as high as 5 cm from the bottom, coming fairly close to the free surface of the flow. This is in agreement with Grass' (1971) observations of boils of fluid on the free surface of flow which appeared to be more pronounced with increasing wall roughness.

In table 5 are also given other statistics associated with the upward paths of

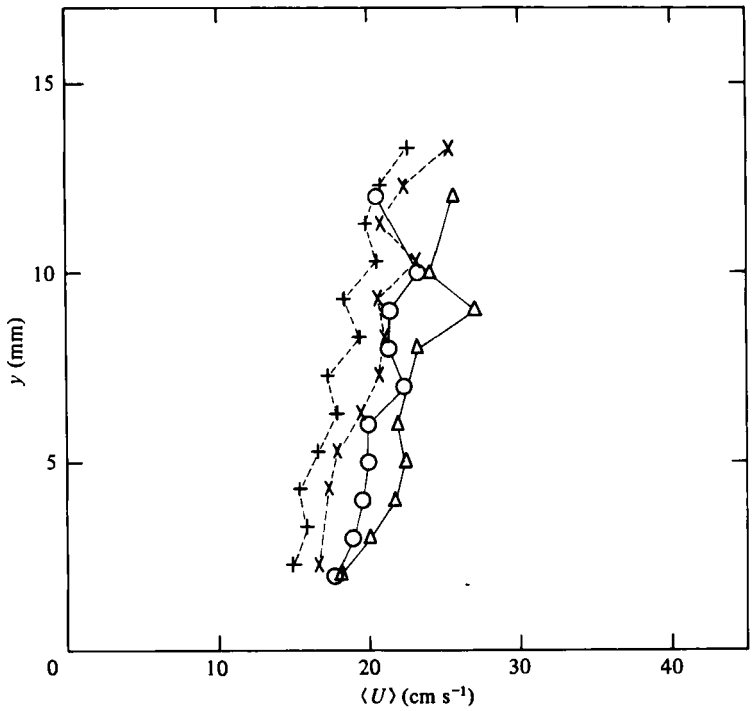

FIGURE 12. Longitudinal velocity data. Mean of the sample of U velocities at a particular depth increment. ○, △, $\langle U \rangle$ corresponding to upward and downward paths, respectively (smooth bottom, particle B); +, ×, $\langle U \rangle$ corresponding to upward and downward paths, respectively (rough bottom, particle D, run $D1$).

particles. From table 5, the streamwise distance travelled by the particle as it traces its upward path appears, on the average, to be slightly smaller in the rough-wall case. Again, from table 5, the mean 'rise' time also appears to be smaller in the rough-wall case. Since the mean 'rise' time of our study corresponds to the mean 'burst duration' of Jackson (1976, table 1) (see §5.1), the latter finding appears to be in agreement with Jackson's result that the mean 'burst duration' decreases with increasing bed roughness. In fact, the reduced 'rise' time reflects the increased ejection velocities in the case of rough-wall flow. These simply scale on the increased shear velocity.

In the case of smooth wall, there appeared to be two types of downward paths (see §3.1): (*a*) one whose y-at-termination is in the wall region ($5 < y^+ < 70$) and (*b*) the other whose y-at-termination is in the outer region ($y^+ > 70$). A similar classification of the downward paths in the rough boundary case is not possible because the smooth-boundary wall region ceases to exist in this case as the roughness Re number, ku_*/ν ($= 81$), falls into the rough boundary category. Instead, in calculating the relevant statistics, all the downward paths observed in the rough-wall tests are considered without any discrimination.

In table 6 are given the statistical properties of streamwise distance X_1 travelled by the particle as it traces its upward and subsequently downward paths. In table 6 similar statistics are also given for the corresponding time T_1. For more information about the path statistics, the reader is referred to Sumer & Deigaard (1979).

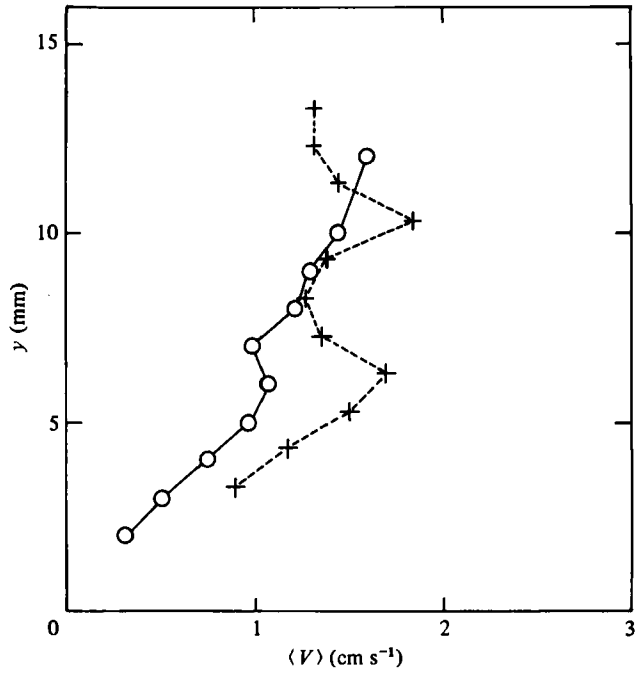

FIGURE 13. Vertical velocity data corresponding to upward paths. Mean of the sample of V velocities at a particular depth increment. ○, smooth bottom (particle B); +, rough bottom (particle D, run $D1$).

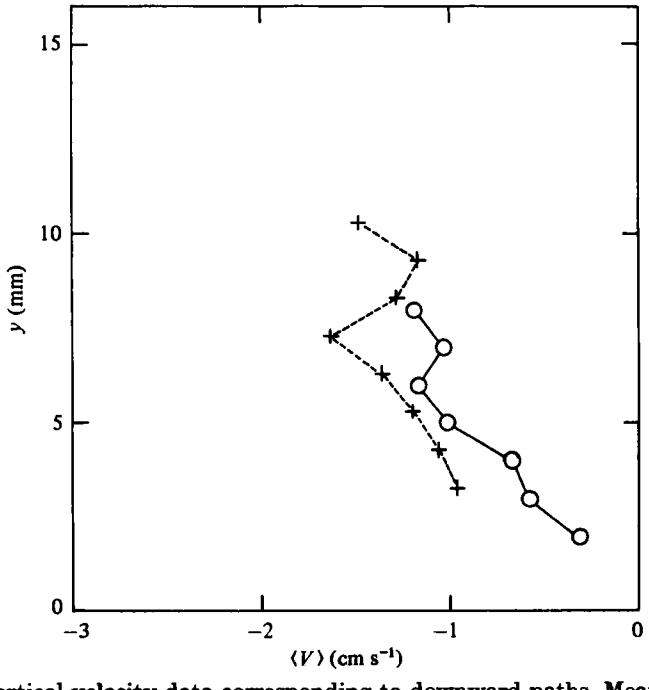

FIGURE 14. Vertical velocity data corresponding to downward paths. Mean of the sample of V velocities at a particular depth increment. ○, smooth bottom (particle B); +, rough bottom (particle D, run $D2$).

4.2. *Particle velocities*

The U- and V-velocity data are plotted in the same manner as in the case of smooth wall (see §3) in figures 12–14 together with the corresponding data of the smooth bottom case. It is apparent that there is a decrease in the longitudinal velocity in the case of rough bottom. This is in accord with the following explanation. Flow very close to the bottom is resisted mainly by viscous shear in the case of smooth boundary whereas, in the case of rough boundary, form drag produces much more effective resistance. Thus flow velocities are expected to decrease with an increase in bed roughness which is confirmed with the present data in figure 12. As far as the particles' upward velocities in the case of rough bottom are concerned, the particles, on the average, rise at velocities appreciably greater than those in the case of smooth bottom; this finding is consistent with Grass' (1971) observations in which entrainment of fluid parcels from near the wall into the flow was observed to be extremely violent in the case of rough wall.

5. Discussion

5.1. *A composite picture of the particle suspension mechanism near the smooth bottom*

The particle suspension mechanism which will be discussed further in this subsection was given in part 1. A brief description of the bursting process was also given in part 1. The reader is therefore referred to the relevant sections of part 1 to keep up the present discussion.

Column 3 of table 3 indicates that particles A and B, the upward motions of which originated in the wall region, reached on the average a y^+ of 125 and 103 respectively (this appears to be in accord with the findings of part 1). Nychas *et al.* (1973) observed, in their experiments, that most of the ejected fluid elements reached a y^+ of 80–100 and some could reach a y^+ of as high as 200 in a single continuous motion. Similarly, Pratury & Brodkey's (1978) recent study showed that the ejected fluid particles travelled up to a y^+ of 100 or more and in some rare cases they travelled up to $300y^+$. Note the close similarity between the present findings and others. On the other hand, the non-dimensionalized mean 'rise' time $\overline{T}u_\infty/h$ was found to be 3·0 for particle A and 2·4 for particle B. This quantity is expected to be in accord with the so-called mean burst duration, which is the time between the onset of lift-up and break-up of a burst; the latter is reported to be $\overline{T}u_\infty/h = 2{\cdot}3$ for smooth boundary data (Jackson 1976, table 2). The agreement between the value reported for fluid particles and that obtained for suspended particles should be noted. Further, the mean streamwise displacement of a particle during its upward motion was found to be $\overline{X}^+ = 2000$ for particle A and 1600 for particle B (column 7 of table 3). These values seem to be in reasonable agreement with the value 1300, which is the reported value of the mean streamwise distance from the onset of lift-up to break-up of a burst (Offen & Kline 1973, p. 112). This new evidence provides further testing of the hypothesis that upward motions of suspended particles whose origins are in the wall region are similar to those of ejected fluid particles.†

† Note that this argument does not apply to particle C as the particle C (being considerably heavier than the other two) reflects no such close similarity. A detailed discussion of the motion of particle C is given in §5.2.

y^+ (1)	No. of total patterns (2)	No. of accepted patterns (3)	% of total patterns in accepted patterns (4)
10	1350	846	63
15	1552	966	62
30	1968	1214	62
45	2211	1303	59

TABLE 7. Percentage of total patterns in accepted patterns in recognizing bursting structures (Wallace *et al.* 1977, table 1).

The velocity data plotted in figures 7 and 8 give additional evidence for the above hypothesis. Firstly, the 'rise' profiles in figure 7 show a defect relative to the 'fall' profiles (particularly in cases of particles A and B); a similar trend was reported by Nychas *et al.* (1973, figure 6) for the actual observed bursting events. Secondly, the agreement between the data on the vertical components of the particle velocity of the present study and the data of other studies obtained from the observations of the actual bursting events also supports the above hypothesis.

There appears to be two types of path patterns associated with the particles which start to rise from the wall region: (*a*) the path pattern which consists of an upward path followed by a downward path, y^+ at the origin of the former, and y^+ at the termination of the latter, both being in the wall region (figure 6), and (*b*) that with a downward path y^+-at-termination of which is in the outer region ($y^+ > 70$). The path pattern of type (*a*) is expected to resemble one complete burst cycle in the Lagrangian sense. Thus information (obtained for particles A and B) given in columns 4, 10 and 12 of table 4 should be expected to be in accord with the available information associated with the burst cycle in the Eulerian sense.

Firstly, we shall look at the information presented in column 4 of table 4 which gives the percentage of the total path patterns in the path patterns resembling a complete burst cycle. Pointing out that it should be possible to recognize coherent structures in turbulent shear flows, Wallace, Brodkey & Eckelman (1977) found that simple signal patterns describe the turbulence structures on the average. The u-signal pattern that Wallace *et al.* used in recognizing the turbulence structures consists of a gradual deceleration from a local maximum followed by a strong acceleration, subject to the criterion that $\max du/dt$ in the acceleration phase be greater than $|\min du/dt|$ in the deceleration phase. Table 7 gives the percentage of the total number of u-signal patterns in the 'accepted' u-signal patterns (used in recognizing the coherent bursting structures in the wall region where most of the turbulence activity takes place) (Wallace *et al.* 1977, table 1). It should be noted that the 'accepted' u-signal pattern resembles one complete burst cycle in the Eulerian sense. Remarkable agreement between the values given in column 4 of table 7 and those in column 4 of table 4 for particle A should be noted. As to particle B, although the agreement seems to be reasonable, slightly higher values should in fact be expected in this case owing to gravity.

Secondly, the non-dimensional mean time $\bar{T}_1 u_\infty/h$ spent by the particle as it traces its subsequent upward and downward paths (see figure 6) was found to be 5·3 for particle A and 4·4 for particle B (table 4). These values are in good agreement with the

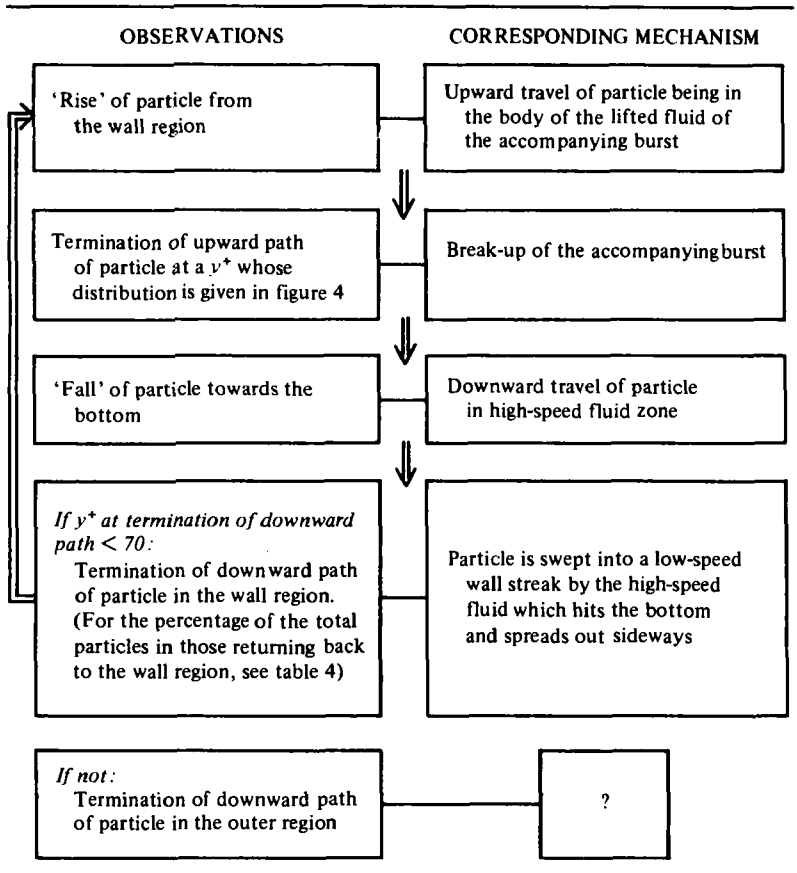

TABLE 8. Summary of observed paths and corresponding mechanism.

reported value of the mean burst periodicity $\bar{T}_1 u_\infty/h = 5$ (see, for example, Jackson 1976, figure 3). Further, the characteristic mean wavelength of the bursting process corresponding to $\bar{T}_1$ can be written as $\bar{X}_1 \simeq u_c T_1$, where u_c is the convection velocity of the larger-scale motions in the wall region. Assuming that u_c is roughly equal to $0{\cdot}8u_\infty$, we obtain from $\bar{T}_1 u_\infty/h = 5$ the following relation (Hinze 1975, pp. 667–684): $\bar{X}_1/h = 4$. The mean streamwise distance travelled by the particle as it traces its subsequent upward and downward paths (see figure 6) is given in column 12 of table 4. As is seen, the values for particles A and B seem to be in reasonable agreement with the value $\bar{X}_1/h = 4$.

On the other hand, from figure 5, in the case of particle A about 72% and in the case of particle B about 84% of the particles in the wall region are ejected from the zone $y^+ < 50$. This finding of the present study is in agreement with the observation of Nychas *et al.* (1973) in which they observed actual bursting events; they report that small-scale fluid ejections originate in $5 < y^+ < 50$. All these new evidences in the above paragraphs provide further testing of the hypothesis that downward motions of suspended particles are similar to those of fluid particles.† Also, the agreement

† Note that this argument does not apply to particle C. The relevant discussion is given in §5.2.

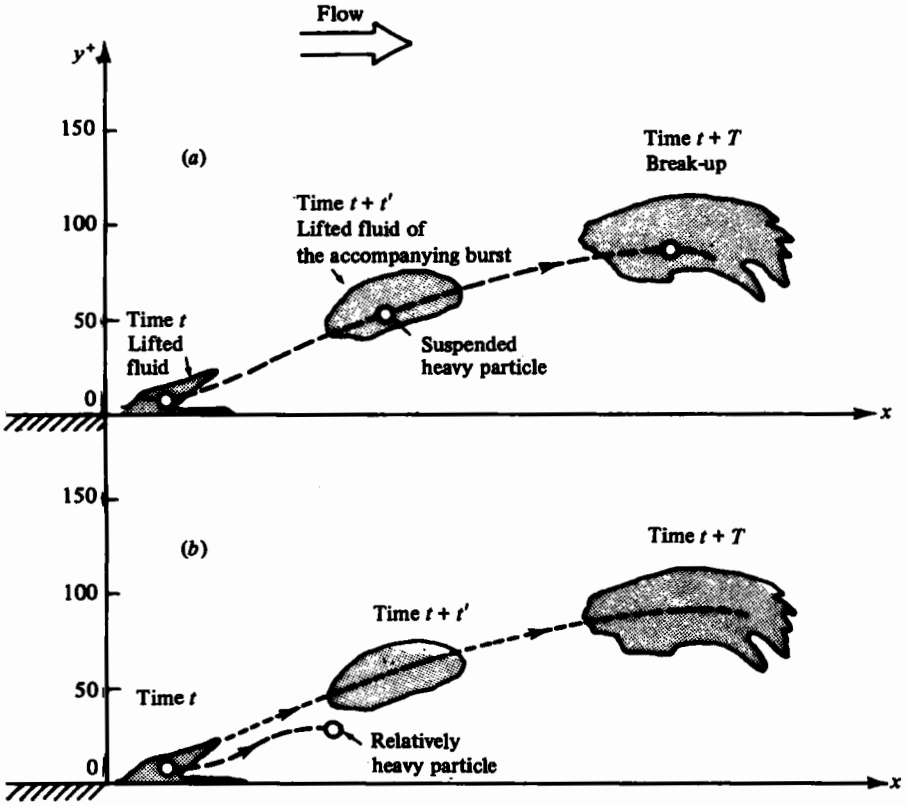

FIGURE 15. (*a*) Schematic view of the side-view motion of suspended heavy particle, and (*b*) that of a relatively heavy particle.

between the particle velocity data and the Brodkey *et al.* data (1974) obtained from the observations of the actual bursting events gives additional support to this hypothesis.

As has been implied above, most of the particles returning back to the wall region are ejected away again from the lower zone ($y^+ < 50$) of the wall region. The mechanism given in part 1 suggests that a particle in the wall region on its way back to the bottom is swept into a low-speed wall streak by the accompanying high-speed fluid. If this argument is correct, the mean transverse displacement of the particle between the instant when the particle enters the lower zone ($y^+ < 50$) of the wall region and the instant when it leaves this zone should be expected to be about $\frac{1}{2}\lambda^+$, where λ^+ is the mean spacing of the low-speed wall streaks and has been reported to be

$$\lambda^+ = \lambda u_*/\nu \cong 100$$

(see, for example, Lee, Eckelman & Hanratty 1974). The mean transverse displacement, $\overline{\Delta Z}$, was predicted in the present study over 44 such paths, 22 of which were taken from the sample space of particle A and the rest from that of particle B; $\overline{\Delta Z}$ was found to be 56 in z^+ units, quite close to the value 50. This evidence as well as others in part 1 (Sumer & Oguz 1978, pp. 122–123) account for particles to be swept into low-speed wall streaks prior to their lift-ups.

Finally, in table 8 is presented a summary of the description of the observed particle

paths and the corresponding stages of the suspension mechanism in the form of a flow-chart (see also figure 15*a* for a schematic description). However, it should be noted that the bursting event is not of constant cycle but rather is highly irregular both in time and in space and is interactive with the similar surrounding structures. Thus it should be borne in mind that particles entrained by one bursting cycle can be intercepted on its way down by similar surrounding structures. It should also be remembered that, along their trajectories, the particles are obviously also subject to the gravitational action, the role of which in the suspension mechanism will be discussed in the next section.

5.2. *Relatively heavy particles*

Particle C (being considerably heavier than particles A and B, but approximately of the same size) was purposely chosen to get an insight into the mechanics of particle motion in the case of relatively heavier particles. Yet particle C is still not heavy enough to move constantly in contact with the bottom by rolling or sliding; rather, it traces a path pattern with a series of short hops, as is seen in figure 3(*b*).

Column 3 in table 3 shows that particle C ejected from the wall region could reach only a y^+ of 54 on the average, a rather low y^+ compared with 125 and 103 for particles A and B respectively. Again, the mean streamwise distance travelled by particle C as it rises comes out to be one third of that travelled by particles A and B (column 7 in table 3). Similarly, the mean 'rise' time (column 13 in table 3) of particle C is considerably smaller than that of particles A and B. Similar considerations apply also to columns 10 and 12 in table 4. On the other hand, figure 7(*c*) indicates that there is an appreciable slip between the fluid and the particle in the case of particle C.†

All these evidences suggest an overshooting effect in the particle's upward path: the particle ejected from the wall region cannot be maintained in the lifted fluid of the accompanying burst but leaves the main body of the lifted fluid due to gravity before the accompanying burst breaks up (see figure 15*b* for a schematic description). Note that the latter coincides with what is conventionally known as the 'crossing-trajectories effect' concept, i.e., a particle falls out of an eddy before the eddy loses its identity.

One would expect that the ejection from the wall region of particle C is due to the same mechanism as that explained in §5.1. Figure 8 supports this argument as there appears no systematic discrepancy in the vertical velocity data of the three particles used in the present work. Figure 5 also gives support for this argument as the y^+ interval, where most of the ejections originate in the case of particle C, appears to be in reasonable accord with those of particles A and B. An additional support comes from figure 9 which shows that there is a consistency between the downward velocity data of particle C and those of particles A and B close to the bottom. All these imply that particle C coming very close to the bottom would finally be swept into a low-speed wall streak.

To sum up, the particle ejected from the wall region falls out of the lifted fluid of the accompanying burst before the burst breaks up, and starts to return back near the

† Figure 7 shows that the heavier the particle is, the more the slip which occurs between the fluid and the particle. Indeed, the relative motion between the fluid and the particle is appreciable in the case of particle C; the mean longitudinal velocity of particle C appears to be about 20 % less than the local mean, while this figure is only 8·5 % for particle B and 6 % for particle A.

bottom. The particle wandering very close to the bottom is finally swept into a low-speed wall streak from where it is ejected again into the flow. This process causes the particle to have a path pattern with a series of short hops as was observed in the case of particle *C* (figure 3*b*).

5.3. *Rough bottom*

The rough bottom results presented in §4 show that particle motions close to a rough wall are very similar in character to those close to a smooth wall. As the flow velocity and flow depth as well as the particle properties were kept almost unchanged in both the smooth- and rough-wall experiments, comparison could also be made in the quantitative sense. The relevant data showed that, although the lifting-up and 'rise' of particles occur more intensely in the case of rough wall, no significant variation in the measured values of various quantities in both cases was observed; indeed, the percentage difference, in the worst case, is less than 15% as to the quantities given in columns 7, 8, 10 and 11 in tables 5 and 6.

The above-mentioned qualitative, even quantitative (partially), similarity between the particle motions close to a rough wall and those close to a smooth wall suggests that the mechanism responsible for particle motions in both cases would be similar – that is, a similar sequence of events (namely, bursting process) seems to occur near a rough boundary as well, which would be the main agent responsible for particle suspension just as in the case of smooth boundary.

It is apparent from figure 12 that a particle, after completing its upward path, travels in a high-speed fluid environment as it travels back to the wall region, since the 'rise' profiles in this figure show a defect relative to the 'fall' profiles. What happens as the high-speed fluid approaches the rough wall seems to be an object of speculation. In the case of smooth wall, high-speed fluid hits the bottom and spreads out sideways; the lateral flows of fluid along the neighbouring sides of two such adjacent high-speed zones of fluid run together, merge each other and are retarded, which in turn gives rise to formation of a new low-speed wall streak. In the case of rough wall, it might be anticipated that the lateral flows of fluid along the neighbouring sides of two adjacent high-speed zones are likely to be retarded by form drag of the roughness elements, which cause the fluid to be trapped between the protrusions, leading to longitudinal localization of the low-momentum fluid and thus causing the disappearance of the smooth-boundary wall streaks. Indeed, Grass (1971) reported that the long twisting streamwise vortices, very apparent close to the smooth boundary during inrush–ejection cycles, were much less conspicuous in the transitional and rough boundary flows in his tests, which implies that low-speed wall streaks cease to exist in the case of rough wall. From these considerations, in the case of rough boundary flow, it seems most likely that the particle, on its way back to the wall region (being in a high-momentum fluid environment), is swept laterally into a localized low-momentum zone from where it is lifted up by a mechanism similar to that in the smooth-wall case.

Because of its direct relevance, the work of Abbott & Francis (1977), which has already been introduced in §1, will be discussed herein in some detail. Abbott & Francis photographed the paths of solid grains in an open water channel with a rough bottom, using a multi-exposure technique. From their observations, they defined the following three modes of particle paths: (*a*) the rolling mode, (*b*) the saltation mode and (*c*) the suspension mode. They plotted the bounds of the aforementioned modes as

a function of the 'transport stage' parameter u_*/u_{*_0}, where u_{*_0} = the 'threshold' shear velocity at which grains just begin to move if they are part of a co-planar, mobile bed. This latter plot shows that the greater the parameter u_*/u_{*_0}, the shorter the time the grain spends in rolling mode as it travels along the channel; particularly for $u_*/u_{*_0} \gtrsim 2$, the percentage of the total time spent in rolling mode is less than 10%. Thus it can be suggested that, for $u_*/u_{*_0} \gtrsim 2$, the grains in Abbott & Francis' experiments were light enough to respond to the 'suspension mechanism' explained in the present work. If this is so, the statistics of the paths of such grains should be in accord with the present 'mechanism'. From figures 3, 4, 12(*a*) and 12(*b*) of Abbott & Francis (1977) we have the following data on the path statistics of such grains:

(I) $h = 4{\cdot}8\,\text{cm}$, $u_*/u_{*_0} = 2{\cdot}8$, $\bar{X}_1 = 20\,\text{cm}$, $\bar{y} = 1{\cdot}9\,\text{cm}$;

(II) $h = 7{\cdot}2\,\text{cm}$, $u_*/u_{*_0} = 3{\cdot}2$, $\bar{X}_1 = 26\,\text{cm}$, $\bar{y} = 2{\cdot}3\,\text{cm}$;

where h = the flow depth, $\bar{X}_1$ = the mean streamwise distance travelled by the grain as it traces its subsequent upward and downward paths and $\bar{y}$ = the mean y at termination of the upward paths in which y is the distance from the bed. The data are designated by the symbols I and II in this paper for convenience. Note that, in Abbott & Francis' experiments, the bottom was covered with rounded pea-gravel 4·8–9·6 mm sieve size which was glued one layer deep to the flume bed. The roughness Reynolds number, ku_*/ν, is estimated to be 700–800 for the preceding data. Also for the same data, the grain size was 8·3 mm and the specific gravity of the grain was 1·24.

When non-dimensionalized with the outer flow parameter h, Abbott & Francis' data give $\bar{X}_1/h = 4{\cdot}1$ and 3·6 for I and II respectively, which is in reasonable accord with our findings (see column 5 of table 6) and in complete agreement with the characteristic wavelength of the bursting process $\bar{X}_1/h = 4$ (see §5). On the other hand, we can make an estimation of the mean time spent by the grain as it traces its subsequent upward and downward paths by using the relation $\bar{T}_1 u_\infty/h \simeq L/(0{\cdot}8h)$ (see §5.1) as no data on this latter quantity have been given in Abbott & Francis (1977). This gives $\bar{T}_1 u_\infty/h = 5{\cdot}2$ and 4·5 for I and II respectively, which again agrees favourably well with the present findings in column 8 of table 6 and the mean burst periodicity $\bar{T}_1 u_\infty/h = 5$.

As to the mean vertical position at termination of upward paths $\bar{y}$, this quantity is expected to scale with the inner flow parameter k, the mean height of roughness elements, drawing an analogy to the smooth-wall case where the same quantity scales with the inner flow parameter ν/u_* (see §3.1 and §5.1). To test this argument, the non-dimensionalized $\bar{y}$s are given in table 9 together with the corresponding findings of the present study, taking k in Abbott & Francis' experiments as $(4{\cdot}8 + 9{\cdot}6)/2 = 7\,\text{mm}$. Although the data presented in the table is far from being adequate both in quality and in quantity, the mean vertical position at termination of upward paths, $\bar{y}$, seems to scale with the inner length scale k, and the agreement between the present data and those of Abbott & Francis is fairly good despite the considerable difference in roughness Reynolds numbers as well as in particle densities.

As Abbott & Francis' path statistics compare fairly well with the present results as well as available information on the bursting structure, one can suggest that the grains in Abbott & Francis' experiments with $u_*/u_{*_0} \gtrsim 2$ are likely to have responded to the 'suspension mechanism' described in the present work.

	$\bar{y}$ (cm)	k (cm)	$\bar{y}/k$
Abbott & Francis (1977)			
I	1·9	0·7	2·7
II	2·3	0·7	3·2
Present study			
Run *D*1	1·07	0·36	3·0
Run *D*2	1·35	0·36	3·7

TABLE 9

Using a new evaluation method for the bursting period T_1, Nakagawa & Nezu (1978) determined $\overline{T}_1 u_\infty/h$ values for their u- and v-records in an open-channel flow where they tried four different bed roughnesses, namely $k_s u_*/\nu = 0$, 9, 48 and 136. They found that $\overline{T}_1 u_\infty/h = 1{\cdot}5 \sim 3$, irrespective of the bed roughness. Although the numerical factor in Nakagawa & Nezu's evaluation is less than the familiar value 5, Nakagawa & Nezu's work is significant in that it shows no sign of dependency of $\overline{T}_1 u_\infty/h$ upon the bed roughness. It is interesting to note that, from the present study and the works by Abbott & Francis (1977) and Nakagawa & Nezu (1978), the mean burst periodicity and the mean characteristic wavelength of the bursting process seem to scale with the outer flow parameters u_∞ and h, irrespective of the bed roughness, as the preceding works cover an extremely wide range of roughness Reynolds number, namely $ku_*/\nu = 0$–800.

6. Conclusions

Using a stereo-photogrammetric technique, observations of the three-dimensional motions of small heavy particles near the bottom of a turbulent open-channel flow were made. The latter showed that the kinematical quantities in connection with particle motions are in accord with those of the bursting process.

The new evidence obtained in the present study provided further support for the mechanism of particle suspension close to the bottom proposed in part 1. A summary of the description of the observed particle paths and the corresponding stages of the mechanism of particle suspension is given in table 8.

In the case when the particle is rather heavy (yet being light enough not to move constantly in contact with the bottom), the present findings suggest that the particle ejected from the near-bottom region falls out of the lifted fluid of the accompanying burst before the latter breaks up. The particle coming near the bottom is finally swept into a low-speed wall streak from where it is ejected again into the flow.

In the rough-bottom case, the observations showed that particle motions close to the bottom are very similar to those in the case of smooth bottom. As the flow velocity and the flow depth as well as the particle properties were kept almost unchanged in both the smooth- and rough-bottom experiments, comparison could also be made in the quantitative sense. No significant change was observed in the measured values of the relevant kinematical quantities. The findings of the rough-boundary experiments suggested that the suspension mechanism given for the smooth-boundary flow could be extended to the rough-boundary case.

However, in the authors' opinion, the following questions associated with the

turbulence structure near a rough wall still remains unanswered: (*a*) Does the lift-up of fluid parcels from the wall occur because of the wakes of the roughness elements? (*b*) If that is so, how could one explain the fact that the mean periodicity of the quasi-cyclic events scales with the outer flow parameters? If not, what is the role of the wakes produced by the roughness elements in the observed flow structure? The authors think that careful observations of flow patterns near a rough wall are needed to achieve a better understanding of what is occurring to the turbulence structure near the rough wall in boundary-layer flows.

The research reported in this paper was supported by the National Council for Scientific Research (Denmark), and the Technical University of Denmark, and partially supported by the Scientific and Technical Research Council of Turkey and the Technical University of Istanbul. The authors would like to express their gratitude to Prof. F. A. Engelund who encouraged the authors in every respect during the course of the investigation.

REFERENCES

ABBOTT, J. E. & FRANCIS, J. R. D. 1977 Saltation and suspension trajectories of solid grains in a water stream. *Phil. Trans. Roy. Soc.* A **284**, 225.

BRODKEY, R. S., WALLACE, J. M. & ECKELMANN, H. 1974 Some properties of truncated turbulence signals in bounded shear flows. *J. Fluid Mech.* **63**, 209.

ENGELUND, F. 1970 A note on the mechanics of sediment suspension. *Basic Res. Prog. Rep. Hydraulic Lab. Tech. Univ. Denmark* **21**, 7.

GRASS, A. J. 1971 Structural features of turbulent flow over smooth and rough boundaries. *J. Fluid Mech.* **50**, 233.

GRASS, A. J. 1974 Transport of fine sand on a flat bed: turbulence and suspension mechanics. *Euromech* 48, *Inst. Hydrodyn. Hydraulic Engng Tech. Univ. Denmark*, p. 33.

HENDERSON, F. M. 1966 *Open Channel Flow*. Macmillan.

HINZE, J. O. 1975 *Turbulence*. McGraw-Hill.

JACKSON, R. G. 1976 Sedimentological and fluid-dynamic implications of the turbulent bursting phenomenon in geophysical flows. *J. Fluid Mech.* **77**, 531.

JACOBI, O. 1979 Photogrammetric tracking of a particle in running water. *Euromech* 120, *Fluid Mech. Dept. Tech. Univ. Denmark*, paper 3.3.

LEE, M. K., ECKELMAN, L. D. & HANRATTY, T. J. 1974 Identification of turbulent wall eddies through the phase relation of the components of the fluctuating velocity gradient. *J. Fluid Mech.* **66**, 17.

LUMLEY, J. L. 1978 Two-phase and non-Newtonian flows. In *Turbulence*, 2nd edn (ed. P. Bradshaw), Topics in Applied Physics, vol. 12, p. 289. Springer.

MONIN, A. S. & YAGLOM, A. M. 1971 *Statistical Fluid Mechanics: Mechanics of Turbulence*, vol. 1. Massachusetts Institute of Technology Press.

NAKAGAWA, H. & NEZU, I. 1977 Prediction of the contributions to the Reynolds stress from the bursting events in open channel flows. *J. Fluid Mech.* **80**, 99.

NAKAGAWA, H. & NEZU, I. 1978 Bursting phenomenon near the wall in open-channel flows and its simple mathematical model. *Memoirs of the Fac. of Engng, Kyoto Univ.* **40** (4), 213.

NYCHAS, S. G., HERSHEY, H. C. & BRODKEY, R. S. 1973 A visual study of turbulent shear flow. *J. Fluid Mech.* **61**, 513.

OFFEN, G. R. & KLINE, S. J. 1973 Experiments on the velocity characteristics of 'bursts' and on the interactions between the inner and outer regions of a turbulent boundary layer. *Dept. Mech. Engng, Stanford Univ. Rep.* MD-31.

PRATURY, A. K. & BRODKEY, R. S. 1978 A stereoscopic visual study of coherent structures in turbulent shear flow. *J. Fluid Mech.* **89**, 251.

SUMER, B. M. & DEIGAARD, R. 1979 Experimental investigation of motions of suspended heavy particles and the bursting process. *Inst. Hydrodyn. & Hydraulic Engng Tech. Univ. Denmark, Lyngby*, Series Paper no. 23.

SUMER, B. M. & OĞUZ, B. 1978 Particle motions near the bottom in turbulent flow in an open channel. *J. Fluid Mech.* **86**, 109.

SUTHERLAND, A. J. 1967 Proposed mechanism for sediment entrainment by turbulent flow. *J. Geophys. Res.* **72**, 6183.

WALLACE, J. M., BRODKEY, R. S. & ECKELMAN, H. 1977 Pattern recognized structures in bounded turbulent shear flows. *J. Fluid Mech.* **83**, 673.